Supporting Information: Hydrogen bonds and van der Waals forces in ice at ambient and high pressures

Biswajit Santra[1], Jiří Klimeš[2,3,4], Dario Alfè[2,4,5,6], Alexandre Tkatchenko[1], Ben Slater[3,4], Angelos Michaelides[2,3,4,*] Roberto Car[7], and Matthias Scheffler[1]

[1]*Fritz-Haber-Institut der Max-Planck-Gesellschaft, Faradayweg 4-6, 14195 Berlin, Germany*

[2]*London Centre for Nanotechnology, University College London, London WC1E 6BT, UK*

[3]*Department of Chemistry, University College London, London WC1E 6BT, UK*

[4]*Thomas Young Centre, University College London, London WC1E 6BT, UK*

[5]*Department of Physics and Astronomy, University College London, London WC1E 6BT, UK*

[6]*Department of Earth Sciences, University College London, London WC1E 6BT, UK*

[7]*Department of Chemistry, Princeton University, Princeton, New Jersey 08544, USA*

In this document we provide brief descriptions of the ice structures and details of the simulations with DFT, vdW corrected DFT, and DMC. Details of additional calculations done to ensure the accuracy of the results in the main manuscript are reported. We also report results illustrating the sensitivity of the lattice energies of certain ice phases to the percentage of Hartree-Fock exchange used in the hybrid DFT calculations.

*angelos.michaelides@ucl.ac.uk

A. Calculations with Density-Functional Theory and van der Waals Correction

1. Polarizability of Isolated Water

The polarizabilities and dipole moments of an isolated water molecule are calculated with the all-electron FHI-aims code [1]. This code uses numeric atom-centered orbitals (NAO) as a basis set and in the polarizability and dipole moment calculations a so-called *tier*3 basis set was used for H and a so-called *tier*4 basis set was used for O. A comparison with DFT, CCSD, and experimental polarizabilities is shown in Table S1.

2. Ice Structures, K points, Codes, Basis Sets Used for Periodic Calculations

The primary structures of all the proton ordered phases of ice are obtained from various scattering experiments [2–7]. Brief descriptions of the unit cells are given in Table S2 and Fig. S1. The structure of proton disordered ice Ih is modelled with the 12 water unit cell proposed by Hamann [8]. This model provides sufficiently accurate bulk properties (lattice energy, volume, and bulk modulus) when compared to those obtained with a much larger unit cell with 96 water molecules (taken from Ref. [9]). Specifically, the lattice energies obtained from 12 and 96 water molecule unit cells are within 1 meV/H_2O and the equilibrium volumes differ only by <0.01 Å^3/H_2O with PBE. For all unit cells the spacing in the **k** point grid in each direction of reciprocal space is within 0.05 Å^{-1} to 0.08 Å^{-1}. Such spacing is sufficient for GGA PBE calculations to ensure fully converged results for each of the ice phases considered. For the hybrid functional (PBE0) calculations a much finer **k** point mesh is required. Fig. S2 shows the convergence of the PBE0 lattice energies with respect to the number of **k** points for all the ice phases. These tests show that doubling the number of **k** points used in the PBE0 calculations compared to what was used for PBE is sufficient to provide total energies converged to within <1 meV/H_2O.

Calculations with PBE, and the PBE0+vdW$^{\mathrm{TS}}$ scheme were performed with the all electron localized basis code FHI-aims [1]. Sufficiently large basis sets (*tier*2 for H and *tier*3 for O) were employed to calculate total energies and to optimize structures. Hybrid *xc* PBE0 calculations were performed with the VASP 5.2 code [10, 11]. The hardest projector augmented wave (PAW) potential together with a 1000 eV energy cut off was employed. With VASP the energy of the water monomer was calculated within a 20 Åcubic cell, which is

sufficiently large to obtain an accurate energy for an "isolated" water monomer. We have ensured that the results obtained from FHI-aims and VASP are in satisfactory agreement. A comparison is shown in Fig. S3.

3. Obtaining Equilibrium Lattice Energies and Volumes

In order to obtain theoretical equilibrium lattice energies (U_0) and volumes (V_0) lattice parameters were varied isotropically in the range of ±6%. This means that the ratios among the lattice parameters are kept fixed to the experimental value. This approximation is reasonable since it has been shown before for ice Ih that the equilibrium c/a ratio is very similar (within ∼0.4%) to the experimental value when calculated with various xc functionals [12]. Also a thorough test was performed here on ice VIII by varying the c/a ratio. This shows an insignificant change of <0.5 meV/H_2O in the U_0 and <0.02 Å^3/H_2O in the V_0 when compared to the results obtained by fixing the c/a ratio at the experimental value. In each unit cell the atoms are fully relaxed with all of the xc functionals (except PBE0+vdW$^{\mathrm{TS}}$) without any symmetry constraints until all forces are less than 0.01 eV/Å. The energy-volume curves of each ice phase with PBE0+vdW$^{\mathrm{TS}}$ were produced by performing single point energy calculations on the PBE0 optimized geometries at different volumes. The resultant energy-volume curves are fitted to the Murnaghan equation of state to obtain equilibrium volumes and lattice energies at zero pressure [13]. Note that the effect of variations of the lattice constants on the lattice energies are small. For example, with the PBE0+vdW(TS) approach at the DMC volumes the lattice energies are -667, -664, and -595 meV/water for ice Ih, II, and VIII, respectively. The corresponding values at the equilibrium PBE0+vdW(TS) lattice constants given in Table I of the main manuscript are -672, -666, -596 meV/water for ice Ih, II, VIII, respectively.

4. Sensitivity of Lattice Energies to Hartree-Fock Exchange

As mentioned in the main manuscript the lattice energies are sensitive to the percentage of Hartree-Fock exchange (HF_x) used in the hybrid functional DFT calculations. We performed these calculations with varying percentages of HF_x because it is not obvious what the most appropriate percentage of HF_x should be for a solid such as ice. Fig. S4 shows the variation

in the lattice energies with increasing percentage of HF_x within the PBE0 form. The most evident trend is that the lattice energies decrease with increasing percentage of HF_x. Note that this trend affects more to the stronger H bonded phases like ice Ih than it does the weaker H bonded phases like ice VIII. So compared to ice Ih the relative stabilities of the high pressure phases increase with the increasing percentage of HF_x. However, the errors in the relative stabilities of the low and high pressure phases remain, and are still large even with 75% HF_x.

5. Zero Point Energy

In order to estimate the role of zero point energies (ZPE) on the relative stabilities of the various phases we calculated ZPEs within the harmonic approximation. The finite displacement method is employed by displacing each atom ±0.005 Å in all 3 spatial dimensions and then the ZPE is calculated by summing over all the phonon frequencies. In Fig. S5 we report the change in the ZPE in the various ice crystals compared to that in an isolated water monomer. It can be seen that in every phase considered there is about 115-125 meV/ H_2O more ZPE than in a gas phase water molecule and that overall ZPE has a minor influence on the relative stability of the various phases. The ZPEs reported here have been obtained with PBE using VASP 5.2 and with a 1000 eV energy cut off.

6. van der Waals Correction

vdW interactions are taken into account by the scheme of Tkatchenko and Scheffler (TS) [14]. The TS scheme is a modified version of the nowadays widely used DFT-D approach [15–18], where a pair-wise C_6/R^6 type vdW interaction with a suitable damping function is added explicitly to the DFT total energies. In this scheme the vdW interaction between a group of atoms (E_{vdW}) is given by,

$$E_{vdW} = \sum_{ij} \frac{C_{6ij}}{R_{ij}^6} f_{damp}(R_{ij}, R_{ij}^0); \;\; f_{damp}(R_{ij}, R_{ij}^0) = \frac{1}{1 + \exp[-d(\frac{R_{ij}}{S_r R_{ij}^0} - 1)]} \quad , \qquad (1)$$

where C_{6ij} are the C_6 coefficients corresponding to atom pair i j, R_{ij} is the distance between the atoms, f_{damp} is the damping function, R_{ij}^0 is the sum of vdW radii of the atoms, d and S_r are two parameters among which d can be fixed to a suitable value (here d=20). As

reported in Ref. [14] S_r parameters are chosen to be 0.94 and 0.96 for PBE and PBE0, respectively. The major improvement in the TS scheme comes from the fact that C_{6ij} and R^0_{ij} coefficients can be derived from DFT electron density and allows subtle variation in the coefficients depending on the molecular environment without empirical fitting. For all the ice phases vdW interaction is added at least up to 40 Å.

B. Diffusion Quantum Monte Carlo Calculations

We have performed diffusion Monte Carlo (DMC) calculations on three phases of Ice: VIII, II and the ambient pressure phase Ih. We used the CASINO code [19] within the fixed node pseudopotential approximation and B-spline basis sets [20]. We have used Dirac-Fock pseudopotentials [21]. The oxygen has a frozen He core with a radius of 0.4 Å and the hydrogen pseudopotential a core radius of 0.26 Å. The trial wavefunctions were of the Slater-Jastrow type, with a single Slater determinant. The single particle orbitals were obtained from DFT-LDA plane-wave calculations usig the PWSCF package [22], using a plane-wave cutoff of 300 Ry, and were re-expanded in B-splines [20].

Initial time step tests were performed on the ice VIII and the ice II structures near their equilibrium volumes, using the primitive cells in both cases. We have performed tests using both the locality approximation [23] and the recent "t-move" scheme of Casula [24]. The t-move scheme gives an upper bound for the exact DMC energy, in the limit of zero time step. The locality approximation is non variational, and therefore can have errors either side of the true energy. These errors are due, in both cases, to the use of non-local pseudopotentials in combination with imperfect trial wavefunctions. The results of the tests are displayed in Fig. S6 (top pannel).

The DMC energies evaluated with the t-move scheme are almost linear in the time step, and they can be easily extrapolated to zero time step. In the case of the locality approximation the behavior of the DMC energy is not linear and it is more difficult to extract the zero time step limit. However, it is clear that with a time step of 0.002 a.u. the energies of both the II and the VIII phases appear to be converged to within ∼5 meV/H_2O. Note, however, that with the same time step of 0.002 a.u. the error in the DMC energies evaluated using the t-move scheme is much larger, and significantly different in the VIII and the II structures. This means that if we wanted to use this scheme we would not be able to rely on cancellation

of errors between the two structures, and we would either have to use a much shorter time step, or perform calculations at a number of different time steps and extrapolate to zero. The other thing to notice about the two schemes is that they converge to different energies, meaning that the t-move and locality errors are fairly large. However, the energy differences between the VIII and the II structures are 17 ± 5 meV/H_2O and 25 ± 5 meV/H_2O with the two schemes respectively, which indicates that the errors due to the use of a non-local pseudopotential do cancel between the two structures. Because of the weaker time step dependence of the DMC energy, we decided to use the locality approximation, and a time step of 0.002 a.u.

The DMC calculations were performed on supercells of dimensions 1×1×1, 2×2×2 and 3×3×2 for the VIII structure, using the zone boundary **k**-point (0.5,0.5,0.5), and 1×1×1 and 2×2×2 for the ice II structure, using the Γ point. For the latter we have also performed one calculation with the zone boundary **k**-point (0.5,0.5,0.5). We have employed the Model Periodic Coulomb (MPC) technique to treat the electron-electron interactions, which helps to significantly reduce DMC size errors [25]. The calculations show that using 2×2×2 supercells in both cases is enough to obtain energies converged to better than 5 meV/H_2O. In the case of ice II structure, the statement of convergence of the 2×2×2 supercell relies on a comparison of the energies obtained with the Γ point and the (0.5,0.5,0.5) point. For the ice Ih structure we only performed calculations using a 2×2×2 supercell. The results for the three ice structures, VIII, II and Ih, are displayed in Fig. S6 (bottom pannel), with the energy zero set to the energy of the isolated water molecule. Structural parameters were obtained by fitting the results to a Birch-Murnaghan equation of state. The results are reported in Table S3.

[1] V. Blum *et al.*, Comp. Phys. Comm. **180**, 2175 (2009).

[2] C. M. B. Line and R. W. Whitworth, J. Chem. Phys. **104**, 10008 (1996).

[3] J. D. Londono, W. F. Kuhs, and J. L. Finney, J. Chem. Phys. **98**, 4878 (1993).

[4] C. Lobban, J. L. Finney, and W. F. Kuhs, J. Chem. Phys. **117**, 3928 (2002).

[5] C. G. Salzmann *et al.*, Science **311**, 1758 (2006).

[6] C. G. Salzmann *et al.*, Phys. Rev. Lett. **103**, 105701 (2009).

[7] W. F. Kuhs *et al.*, J. Chem. Phys. **81**, 3612 (1984).

[8] D. R. Hamann, Phys. Rev. B **55**, R10157 (1997).

[9] D. Pan *et al.*, Phys. Rev. Lett. **101**, 155703 (2008).

[10] G. Kresse and J. Hafner, Phys. Rev. B **47**, 558 (1993).

[11] G. Kresse and J. Furthmüller, Phys. Rev. B **54**, 11169 (1996).

[12] P. J. Feibelman, Phys. Chem. Chem. Phys. **10**, 4688 (2008).

[13] F. Birch, Phys. Rev. **71**, 809 (1947).

[14] A. Tkatchenko and M. Scheffler, Phys. Rev. Lett. **102**, 073005 (2009).

[15] R. Ahlrichs, R. Penco, and G. Scoles, Chem. Phys. **19**, 119 (1977).

[16] S. Grimme, J. Comput. Chem. **25**, 1463 (2004).

[17] P. Jurečka, J. Černý, P. Hobza, and D. R. Salahub, J. Comput. Chem. **28**, 555 (2007).

[18] Q. Wu and W. Yang, J. Chem. Phys. **116**, 515 (2002).

[19] R. J. Needs *et al.*, J. Phys.: Condensed Matter **22**, 023201 (2010).

[20] D. Alfè and M. J. Gillan, Phys. Rev. B **70**, 161101 (2004).

[21] J. R. Trail and R. J. Needs, J. Chem. Phys. **122**, 014112 (2005); *ibid* J. Chem. Phys. **122**, 174109 (2005).

[22] P. Giannozzi *et al.*, J. Phys.:Cond. Matt. **21** 395502 (2009).

[23] L. Mitáš *et al.*, J. Chem. Phys. **95**, 3467 (1991).

[24] M. Casula, Phys. Rev. B **74**, 161102 (2006).

[25] L. M. Fraser *et al.*, Phys. Rev. B **53**, 1814 (1996).

[26] J. R. Hammond *et al.*, J. Chem. Phys. **131**, 214103 (2009).

[27] G. D. Zeiss and W. J. Meath, Mol. Phys. **30**, 161 (1975).

[28] S. A. Clough *et al.*, J. Chem. Phys. **59**, 2254 (1973).

[29] H. J. Monkhorst and J. D. Pack, Phys. Rev. B **13**, 5188 (1976).

[30] E. Whalley, J. Chem. Phys. **81**, 4087 (1984).

[31] K. Röttger, A. Endriss, J. Jhringer, S. Doyle, and W. F. Kuhs, Acta Cryst. **B50**, 644 (1994).

[32] A. D. Fortes, I. G. Wood, M. Alfredsson, L. Vočadlo, and K. S. Knight, J. Appl. Cryst. **38**, 612 (2005).

[33] G. H. Shaw, J. Chem. Phys. **84**, 5862 (1986).

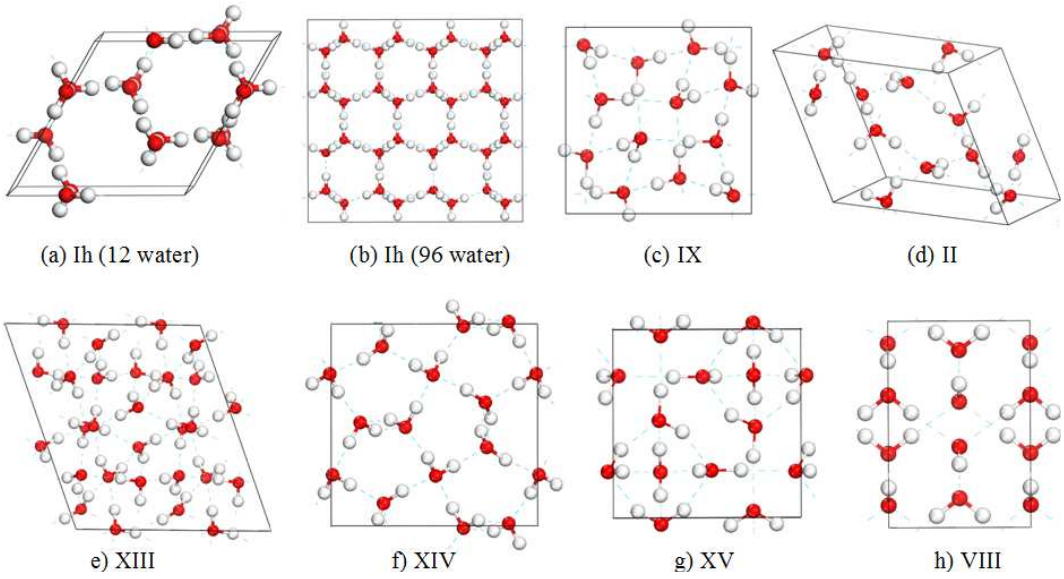

FIG. S1. Unit cells of the ice phases studied are shown here. Brief descriptions are given in Table S2. The red spheres are oxygen atoms and the white spheres are hydrogen atoms.

TABLE S1. Isotropic polarizability (a.u.), anisotropic polarizability (a.u.), and dipole moment (Debye) of an isolated water molecule with different methods. CCSD and CCSDT polarizabilities are taken from Ref. [26], the experimental polarizability is taken from Ref. [27], and the experimental dipole moment is taken from Ref. [28].

	PBE	PBE0	CCSD	CCSDT	Expt.
Isotropic Polarizability	10.66	9.69	9.54	9.55	9.63
Anisotropic Polarizability	0.23	0.50		0.59	
Dipole Moment	1.80	1.85	1.86		1.855

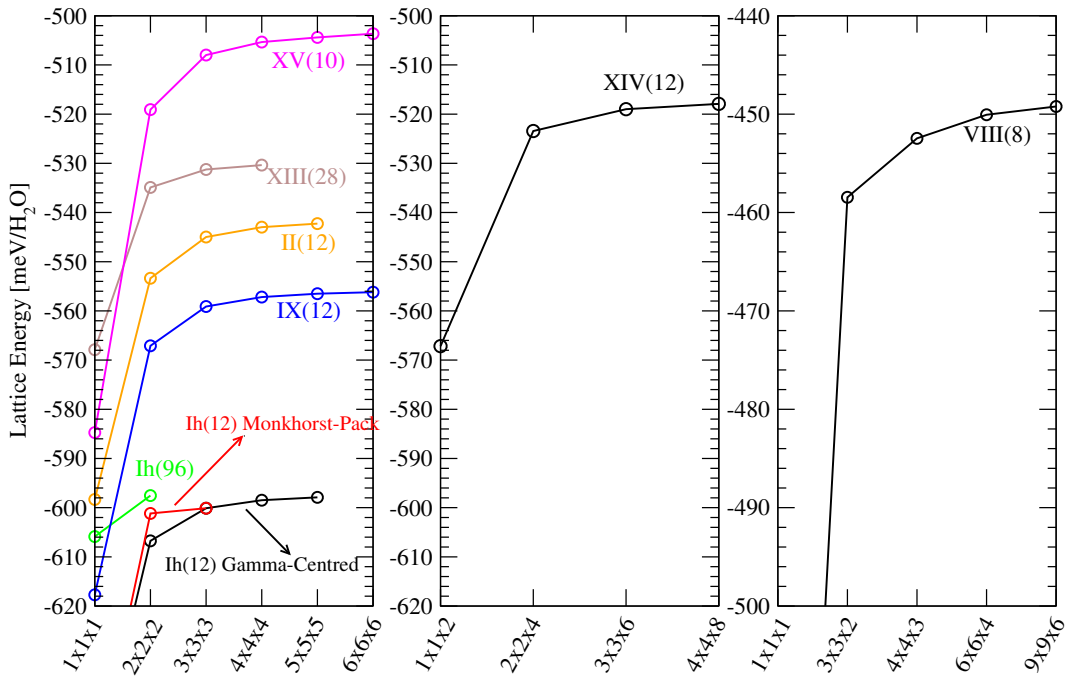

FIG. S2. Convergence of lattice energy with respect to number of **k** points used for the PBE0 calculations for all the ice phases. The values given in parenthesis represent the number of water molecules in the unit cell. The number of **k** points used for the reported results are given in Table S2.

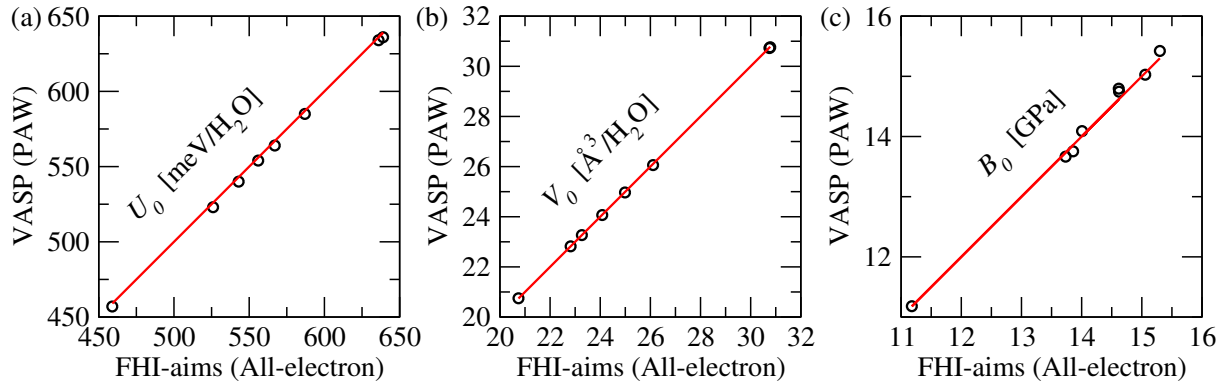

FIG. S3. Comparison of the results obtained from the all electron code FHI-aims and the PAW code VASP for the equilibrium (a) lattice energies (U_0), (b) volumes (V_0), and (c) bulk moduli (B_0) of all ice phases studied here (calculated with PBE). For all the phases studied here the mean differences between FHI-aims and VASP are 2.5 meV/H_2O for U_0, 0.02 Å^3/H_2O for V_0, and 0.09 GPa for B_0.

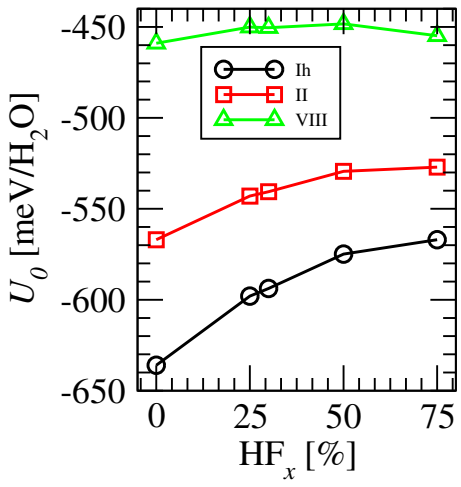

FIG. S4. Lattice energies of ice Ih, II, and VIII as a function of the percentage Hartree-Fock exchange (HF_x) used in the hybrid DFT calculations. 25% HF_x corresponds to the PBE0 functional and 0% HF_x refers to the PBE functional.

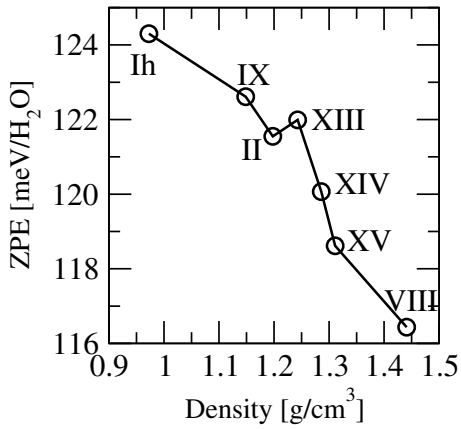

FIG. S5. Excess zero point energy (ZPE) of the water molecules in the various ice phases as a function of the PBE equilibrium densities of the various ice phases. Zero point energies are calculated with PBE *xc* at the PBE equilibrium structures.

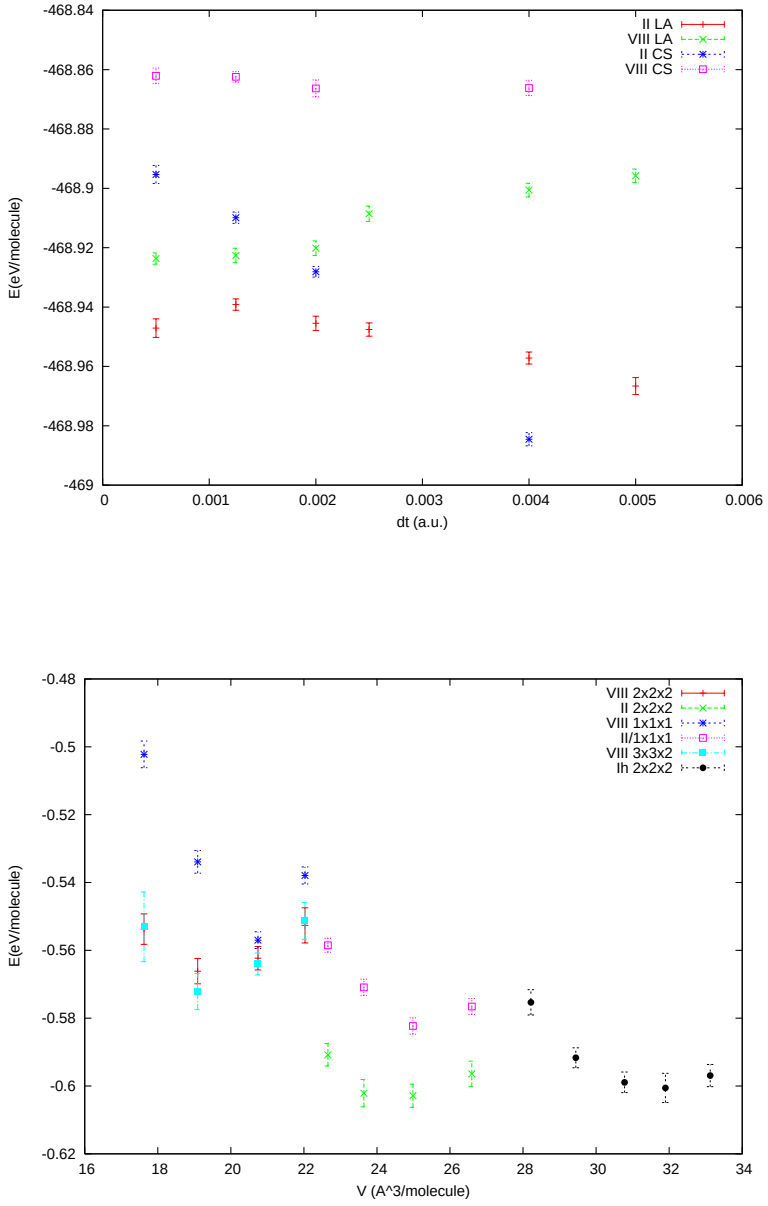

FIG. S6. Top pannel: DMC energies for the ice II (red diamonds and blue stars) and the ice VIII (green crosses and purple squares) structures as a function of time step, using the locality approximation (referred to as LA) [23] (red diamonds and green crosses) or the Casula scheme (referred to as CS) [24] (blue stars and purple squares). Bottom pannel: DMC lattice energies for the ice VIII, II and Ih phases as a function of volume using various supercell sizes.

TABLE S2. For the structures of all ice phases studied here the references (Ref.), the type of Bravais lattice, the symmetry space group, lattice parameters (in Å and degrees), number of water molecules in the unit cells (N_{H_2O}), and the number of **k** points used for the simulations (for the PBE and PBE0 functionals) are given here. Gamma centred **k** points were used only for PBE0 calculations of Ih-12 and for the others a Monkhorst-Pack [29] mesh of **k** points was employed.

Ice	Ref.	Bravais Lattice	Space Group	Lattice Parameters	N_{H_2O}	**k** points	
						PBE	PBE0
Ih-12	[8]	Hexagonal	$P6_3cm$	a=b=7.78, c=7.33, γ=60	12	2×2×2	4×4×4
Ih-96	[9]	Hexagonal		a=13.26, b=15.31, c=14.43	96	1×1×1	2×2×2
IX	[3]	Tetragonal	$P4_12_12$	a=b=6.69, c=6.71	12	2×2×2	4×4×4
II	[4]	Trigonal	$R\bar{3}$	a=b=c=7.71, α=113.1	12	2×2×2	4×4×4
XIII	[5]	Monoclinic	$P2_1/a$	a=9.24, b=7.47, c=10.29, β=109.1	28	2×2×2	4×4×4
XIV	[5]	Orthorombic	$P2_12_12_1$	a=8.35, b=8.13, c=4.08	12	2×2×4	4×4×8
XV	[6]	Triclinic	$P\bar{1}$	a=6.23, b=6.24, c=5.79, α=90.1, β=γ=89.9	10	3×3×3	5×5×5
VIII	[7]	Tetragonal	$I4_1/amd$	a=b=4.65, c=6.77	8	3×3×2	6×6×4

TABLE S3. DMC equilibrium volumes (V_0), bulk moduli (B_0), and lattice energies (U_0) of the ice VIII, II, and Ih phases. Calculated DMC properties are reported at 0 K without ZPE corrections. Experimental values at or near 0 K are given for comparison. Note that in the experimental lattice energy ZPE contributions have been removed.

	Ice	Supercell	V_0 (Å^3/H_2O)	B_0 (GPa)	U_0 (meV/H_2O)
DMC	VIII	1×1×1	20.43±0.04	34.8±0.2	-556±10
	VIII	2×2×2	19.55±0.05	17.6±0.2	-570±5
	VIII	3×3×2	19.46±0.02	23.8±0.5	-575±5
Expt.	VIII		20.09[a]		-577[a]
DMC	II	1×1×1	25.3±0.3	22.2±0.6	-585±5
	II	2×2×2	24.7±0.2	20.1±0.4	-609±5
Expt.	II		24.97[a]	12.1[c]	-609[a]
DMC	Ih	2×2×2	31.69±0.01	18.3±0.1	-605±5
Expt.	Ih		32.05[b]	9.5[d]	-610[a]

[a]Ref. [30]; [b]Ref. [31]; [c]Ref. [32]; [d]Ref. [33]